Mon. Not. R. Astron. Soc. **000**, 1–8 (XXXX) Printed 3 September 2015 (MN LaTeX style file v2.2)

arXiv:1509.00738v1 [astro-ph.HE] 2 Sep 2015

The structure of the X-ray absorber in Mrk 915 revealed by *Swift*

P. Severgnini[1]⋆, L. Ballo[1], V. Braito[1,2], A. Caccianiga[1], S. Campana[1],
R. Della Ceca[1], A. Moretti[1] and C. Vignali[3]
[1] *INAF–Osservatorio Astronomico di Brera, via Brera 28, I-20121 Milano, Italy*
[2] *Department of Physics, University of Maryland, Baltimore County, Baltimore, MD 21250, USA*
[3] *Dipartimento di Fisica e Astronomia, Università degli Studi di Bologna, Viale Berti Pichat 6/2, I-40127 Bologna, Italy*

Accepted 2015 August 10. Received 2015 June 22, in original form 2015 April 2

ABSTRACT

In this paper we present the results obtained with a monitoring programme (23 days long) performed with *Swift*-XRT on the local Seyfert galaxy Mrk 915. The light-curve analysis shows a significant count rate variation (about a factor of 2–3) on a time-scale of a few days, while the X-ray colours show a change in the spectral curvature below 2 keV and the presence of two main spectral states. From the spectral analysis we find that the observed variations can be explained by the change of the intrinsic nuclear power (about a factor of 1.5) coupled with a change of the properties of an ionized absorber. The quality of the data prevents us from firmly establishing if the spectral variation is due to a change in the ionization state and/or in the covering factor of the absorbing medium. The latter scenario would imply a clumpy structure of the ionized medium. By combining the information provided by the light curve and the spectral analyses, we can derive some constraints on the location of the absorber under the hypotheses of either homogeneous or clumpy medium. In both cases, we find that the absorber should be located inside the outer edge of an extended torus and, in particular, under the clumpy hypothesis, it should be located near, or just outside, to the broad emission line region.

Key words: galaxies: active – galaxies: individual: Mrk 915 –X-rays: galaxies.

1 INTRODUCTION

There is now a general consensus that active galactic nuclei (AGN) are powered by accretion of matter on to a supermassive ($>10^6$ M$_\odot$) black hole (SMBH). According to the unified model of AGN (Antonucci 1993), an obscuring optically thick medium composed by dust and gas arranged in a torus-like geometry is present around the nuclear engine. However, the structure, size and composition of this circumnuclear medium are still matter of debate and are topics of several studies carried out at different wavelengths (Bianchi, Maiolino, & Risaliti 2012). Important constraints on the physical properties of the circumnuclear medium have been recently provided by the study of the absorption variability, which is almost ubiquitous in bright absorbed AGN (Risaliti et al. 2002). X-ray absorbing column density ($N_{\rm H}$) has been observed to vary by a factor of 10 or more over a few years. The observed $N_{\rm H}$ variability on this scale ruled out the simplest physical configuration of a homogeneous absorber, giving upper limits on the distance of the latter by the central SMBH. Subsequent X-ray observational campaigns detected significant variability on a handful of AGN on very short time-scale (day or week) giving the possibility to investigate the X-ray properties of the circumnuclear medium down to sub-parsec scale. The emerging picture is that multiple neutral and ionized absorbers co-exist around the central SMBH, located at different distances from it. So far the best characterization of the physical parameters of the X-ray absorbers has been possible for the AGN in NGC 1365, which has been monitored several times in the last few years with *Chandra*, *XMM-Newton* and *Suzaku*. This source changes from Compton-thick ($N_{\rm H}\geqslant10^{24}$ cm^{-2}) to Compton-thin ($N_{\rm H}\sim10^{23}$ cm^{-2}) state on time-scales from weeks (Risaliti et al. 2005) to hours or days (Risaliti et al. 2007, 2009). One of the main results is that the X-ray absorber has the physical properties typical of the clouds responsible for the emission of the broad lines in the optical/UV spectrum, i.e. the broad-line emission region (BLR), located at a distance of hundreds of gravitational radii from the central SMBH. Recently it has been proposed that the

---

⋆ E-mail: paola.severgnini@brera.inaf.it

© XXXX RAS

long-term variability of the X-ray absorber in NGC 1365 could be due to the variation of the ionized X-ray wind, that is responding to the changes in the accretion rate (Connolly, McHardy, & Dwelly 2014). High spectral resolution data show that this wind is located within the variable soft X-ray absorber and is composed by two (or even three) zones with different ionization levels. In particular, the lowest ionization zone of this wind could be responsible for the absorption variability that is observed in this source below 2 keV (Braito et al. 2014).

By exploiting the *Swift* X-ray Telescope (hereafter XRT; Burrows et al. 2005) archive, we recently started a project aimed at studying, on a larger statistical basis, the physical properties of the X-ray absorbers in AGN. We started from the 70 months all-sky survey *Swift*-BAT catalogue (Baumgartner et al. 2013) in the 20–150 keV and the 66-month Palermo BAT Catalogue[1] (see also Cusumano et al. 2010). We considered only those sources with a secure optical AGN counterpart and with XRT observations already available before the end of 2012. For each source, we adopted a daily binning of the XRT data and we searched for statistically significant variations of the X-ray colours on different time-scales (from months to years, see Ballo et al. 2015). Following this method, we selected five new candidates for variable absorbers. One of the most interesting is the local Seyfert galaxy Mrk 915. The archival XRT data used to select this source unveiled a dramatic count rate and 'X-ray colour' variability on a minimum time-scale of 1 month. The 0.3–10 keV count rate increases by a factor of 3 and, at the same time, the spectral shape becomes dramatically softer, showing a variability of a factor of 2.4 and 3 in the [2–10 keV]/[0.3–2 keV] and [4–10 keV]/[0.3–4 keV] count rate ratios, respectively. As discussed in Ballo et al. (2015), this behaviour suggests that a change in the properties of the X-ray obscuring circumnuclear medium (i.e. column density, covering factor or ionization state) probably occurred between the archival XRT observations. However, the low statistical quality of these data prevented us from performing a proper spectral analysis and to discern among the possible causes of the observed variation. With the goal of obtaining higher quality data on a shorter time-scale, we performed a daily XRT monitoring on this source during a period of ∼3 weeks. This paper aims at providing a first characterization of the putative variable absorber.

The paper is structured in the following way: the main optical properties of Mrk 915 are reported in Section 2, while the analysis of the XRT data obtained during the daily monitoring are presented in Section 3 (light-curve analysis and spectral analysis, Sections 3.1 and 3.2, respectively). The main results obtained are discussed in Section 4 and the conclusions are summarized in Section 5.

Throughout the paper we assume a flat ΛCDM cosmology with H_0=71 km s^{-1} Mpc^{-1}, Ω_Λ=0.7 and $\Omega_{\rm M}$=0.3.

2 MRK 915

Mrk 915 is a local (z=0.024) spiral galaxy (PA∼166^o) with evident dust lane structures seen crossing the central source in its WFPC2 image (Malkan, Gorjian, & Tam 1998) and hosting an SMBH of $M_{\rm BH}$=(0.6-1.8)×10^8 M$_\odot$ (Bennert et al. 2006). The value of the axis ratio (0.54 and 0.83 reported by Keel 1996 and Muñoz Marín et al. 2007, respectively) indicates that the disc of the galaxy is inclined with respect to the line of sight by about 35^o-57^o. Assuming both galaxy's disc and AGN's torus to be co–planar and an half-opening angle of the torus of about 60^o, our line of sight intercepts or grazes the low–density outer regions of the torus.

Table 1. Mrk 915: XRT monitoring observation log. The observations are ordered on the basis of the observation start date.

Obs. ID	Obs. start date	Net counts [0.3–10 keV]	Net exp. time [s]
00035169003	2014-09-10	638	7367
00035169004	2014-09-11	621	7060
00035169005	2014-09-15	344	4453
00035169006	2014-09-17	1359	13130
00035169007	2014-09-18	437	3629
00035169008	2014-09-21	2563	13190
00035169009	2014-09-23	693	4105
00035169013	2014-09-27	160	1171
00035169014	2014-09-27	61	719
00035169011	2014-09-29	935	10280
00035169015	2014-10-02	993	5369
00035169016	2014-10-02	1216	5314

From the optical point of view, Mrk 915 has been spectroscopically classified as an intermediate Seyfert[2] galaxy showing significant spectral variations. In particular, the broad components of the Hα and Hβ emission lines are clearly detected in some observations, while they are completely absent in others. As a consequence, the source has been classified in different ways, from Seyfert 1.5 to Seyfert 1.9, depending on the presence/intensity of the broad components at the time of the observations (Goodrich 1995; Bennert et al. 2006; Trippe et al. 2010). The origin of this spectral variability is still unclear. Goodrich (1995) tentatively suggested that the observed variation was due to a change in reddening (ΔE$_{B-V}\geqslant$0.53 mag, derived by comparing the Hα fluxes in the two observations) produced by dusty clouds passing close, but outside, the bulk of the BLR. Alternatively, the observed spectral variability could be due either to a change in the nuclear photoionizing continuum or to a combination of continuum and reddening variation. At the moment, it is not possible to discriminate among the various scenarios (Trippe et al. 2010).

Independently of the origin of this spectral variability, a reddening of the order of E$_{B-V}$∼0.3-0.5 mag seems to be always present and it affects both the kpc-distance regions, i.e. the narrow-line emission regions (NLR), and the innermost nucleus. This reddening is most probably attributed to the presence of dust lanes as seen crossing the central source in its WFPC2 image (Muñoz Marín et al. 2007).

---

[1] http://bat.ifc.inaf.it/bat_catalog_web/66m_bat_catalog.html

[2] A Seyfert galaxy with broad emission line components weaker than those usually observed in Seyfert 1 galaxies (Whittle 1992).

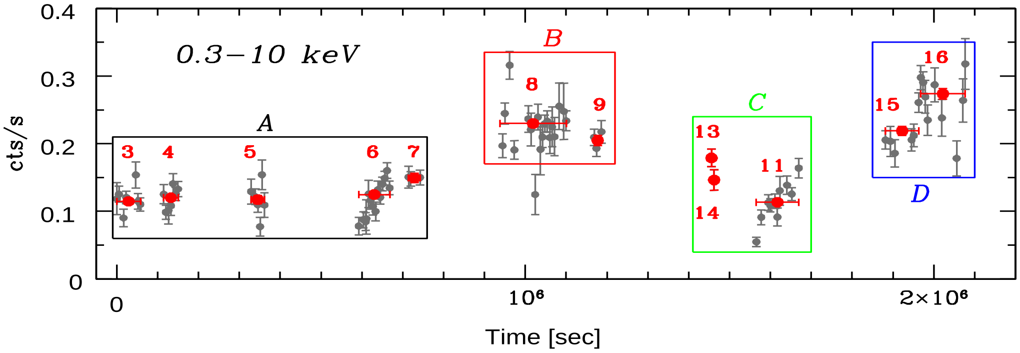

Figure 1. XRT light curve in the total 0.3–10 keV band, obtained by binning the data per snapshot (small dots, grey in the electronic version) and per observation (big dots, red in the electronic version). With respect to the observed net counts reported in Table 1, data points are corrected for technical issues (i.e. bad pixels/columns, field of view effects, pile-up and source counts landing outside the extraction region) following the receipts discussed by Evans et al. (2007) and Evans et al. (2009). Numbers mark the one/two last digital numbers of the relevant observation ID (see Table 1). Error bars mark 1σ uncertainties. The light curve is divided in time intervals marked by different boxes and capital letters (see Section 3.2). We note that the only point in the *B* time range with a count rate lower than 0.2 has a very short exposure time (∼180 s). Although it is above the minimum exposure time considered here (i.e. 150 s), this point has a signal–to–noise ratio lower than 5.

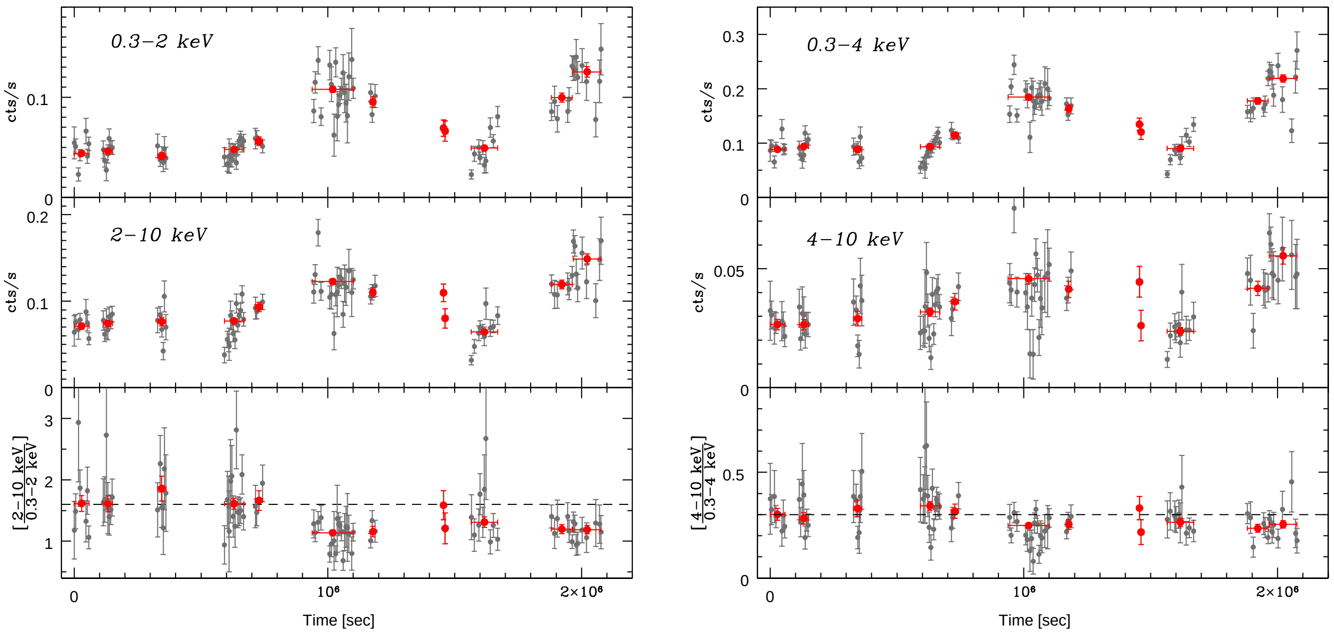

Figure 2. Left panels, from top to bottom: 0.3–2 keV and 2–10 keV count rates and [2–10 keV]/[0.3–2 keV] ratio. Right panels, from top to bottom: 0.3–4 keV and 4–10 keV count rates and [4–10 keV]/[0.3–4 keV] ratio. Dashed lines represent the ratios normalized to the first observation. Symbols are the same as those used in Fig. 1 and data points are corrected for the same technical issues.

3 DAILY/WEEKLY X-RAY MONITORING

The data presented here are relative to a monitoring programme composed by 12 new XRT observations awarded during fall 2014 (*Swift Cycle–10* and ToO observations, P.I. Severgnini). These observations, covering ∼23 days, for a total on source exposure time of ∼76 ks, were performed with XRT in the standard PC-mode. The observation log is reported in Table 1. The source appears point–like in the XRT image and we do not find any significant evidence of pile-up.

3.1 Light curves

Each light curve, described below, has been created by using the *Swift*-XRT data products generator[3] developed by

---

[3] http://www.swift.ac.uk/user_objects/

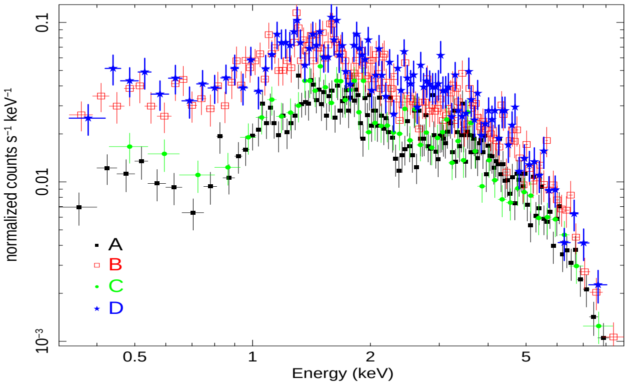

Figure 3. XRT spectra relevant to the time binning defined in Fig. 1. In the electronic version, the spectra are colour-coded as the boxes in Fig. 1.

the UK *Swift* Science Data Centre and based on the Swift software and FTOOLS guide. The effects of the damage to the CCD and automatic readout-mode switching are appropriately handled; details on the light-curve code can be found in Evans et al. (2007) and Evans et al. (2009).

Figs 1 and 2 show the XRT light curves in five different energy bands (0.3–10, 0.3–2, 0.3–4, 2–10 and 4–10 keV). We choose to bin the data per spacecraft orbit (i.e snapshot, grey small dots in Figs 1 and 2). We considered only those snapshots longer than 150 seconds, which guarantee a signal-to-noise ratio on each point equal or greater than 5. In each panel, we plot also the light curves obtained by binning the data per observation (i.e. obs. ID, big red dots in Figs 1 and 2). Over the length of the observing monitoring programme ($\sim$23 days), the light curves are not constant at 99.9 per cent confidence level (χ^2 test).

During the first three observations, spanning $\sim3.6\times10^5$ s (i.e. 4.2 days), the snapshot 0.3–10 keV count rates are randomly distributed around $\sim$0.12 counts s^{-1}. Later, a clear increase in the count rate is visible, reaching its maximum in about 3.5×10^5 s (i.e. $\sim$4 days). In these four days, the count rate increased by a factor $\sim$2–3 when we consider the obs. ID time binning. About 2 days later, the count rate decreased by the same amount and then immediately increased again, reaching the highest intensities observed during this monitoring ($\sim$0.3 counts s^{-1}).

The increasing/decreasing factor is not the same in all bands: in the softer bands (0.3–2 keV and 0.3–4 keV) the count rate variation is higher with respect to that in the complementary harder bands (2–10 keV and 4–10 keV, respectively). This is visible also inspecting the flux ratios ([2–10 keV/0.3–2 keV] and [4–10 keV/0.3–4 keV]) reported in the bottom panels of Fig. 2. In these panels, the dashed lines are normalized to the first observation. This behaviour suggests that, besides the possible flux variation of the primary emission, there could be another mechanism producing different intensity variations in different energy bands. This mechanism should affect mainly the softer energy ranges.

3.2 X-ray spectral analysis

The aim of this section is to investigate, from a spectral point of view, the changes observed in the light curves of Mrk 915 during the X-ray monitoring. To this end, following the total (0.3–10 keV) light curve, we divided the XRT data in four main time bins on the basis of the average count rate value of each observation. They are shown in Fig. 1, where we mark each bin with boxes and capital letters. The A and C bins are composed by observations with a net count rate lower than $\sim$0.2 counts s^{-1}, while B and D correspond to observations with a net count rate higher than $\sim$0.2 counts s^{-1}. For each bin, we extracted the spectrum by using circular regions centred on the X-ray source position with a radius $\sim$50 arcsec (i.e. $\sim$20 pixel, which corresponds to an Encircled Energy Fraction of $\sim$90 per cent; Moretti et al. 2005). The background spectra have been extracted from source-free circular regions close to the object with an area about 9 times larger. Spectral reduction was performed using the standard software (HEADAS software, v6.15 and the most updated CALDB version[4]) and following the procedures described in the instrument user guide[5]. The spectra have been binned in order to have at least 20 counts per energy channel (see Fig. 3) and analysed using the XSPEC 12.8.1 package.

As evident from Fig. 3, the data have two by two (A with C and B with D) very similar spectral shape, confirming the presence of two different spectral states of the source, as already highlighted by the light curve and X-ray colours. A visual inspection of the figure is sufficient to notice that most of the spectral variation among these two states is below 2–3 keV. In order to improve the statistics, we combined the data sets with similar spectral shape (A with C and B with D) by obtaining a low and a high–state spectrum (hereafter called AC and BD, respectively).

We also considered the *Swift*–BAT spectrum of Mrk 915 retrieved by the 70 month *Swift*-BAT Catalogue[6] (Baumgartner et al. 2013). This spectrum provides the average spectral properties of the source above $\sim$15 keV. Due to the significant variability of Mrk 915, we did not fit the XRT and BAT spectra simultaneously. We used the BAT spectrum to derive the average value of the spectral slope of the primary AGN emission. By fitting the BAT data with a simple power-law component, we found a best-fitting value of Γ=1.7$\pm$0.2. In the spectral analysis of the XRT data (described in details below), we first fitted simultaneously the two main states keeping Γ tied. Also in this case we found: Γ = 1.7$\pm$0.2. The same value and uncertainties are obtained when Γ is allowed to vary between the states. Thus, considering the statistic of the present data, we decided to keep it fixed to the best-fitting value while investigating the origin of the variability.

As a starting point, we assumed the presence of three absorbing components. The first one (*phabs* component in XSPEC) refers to the Galactic hydrogen column density along the line of sight (Kalberla et al. 2005). The second one (*zphabs* component in XSPEC) accounts for the absorption due to the dust lane structures at the redshift of the source. Indeed, as discussed in Section 2, the primary emission from the Mrk 915 nucleus intercepts dust lane structures that produce an optical extinction of E_{B-V}=0.3–0.5 mag (Bennert et al. 2006; Trippe et al. 2010). The presence of

---

[4] http://heasarc.gsfc.nasa.gov/FTP/caldb

[5] http://heasarc.nasa.gov/docs/swift/analysis/documentation

[6] http://swift.gsfc.nasa.gov/results/bs70mon/

Table 2. Best-fitting values obtained by applying to the low- and high-state spectra of Mrk 915 the following model: *phabs*×(*zphabs*×*zxipcf* ×*zpowerlw*) with Γ fixed to 1.7 (χ^2/d.o.f.=362.99/403).

State	${N_{\rm H}}^a_{\rm neutral}$	${N_{\rm H}}^b_{\rm ionized}$	CF^c	log(ξ)^d	$A_{\rm p}^e$	$F_{(2-10{\rm keV})}{}^f$	$L_{(2-10{\rm keV})}{}^g$
AC	$0.08^{+0.03}_{-0.06}$	1.86±0.20	0.96±0.03	0.68±0.13	1.98±0.01	0.67	0.98
BD	0.08^h	2.09±0.35	$0.86^{+0.07}_{-0.05}$	$1.14^{+0.14}_{-0.24}$	3.06±0.01	1.07	1.52

Notes: The uncertainties, reported at the 90 per cent confidence level for one parameter of interest, have been estimated by freezing the $N_{\rm H neutral}$ to the best-fitting value.
^{a} Column density of the neutral absorber associated with dust lane structures, in units of 10^{22} cm^{-2}. This parameter is forced to be equal in both states. ^{b} Column density of the ionized absorber, in units of 10^{22} cm^{-2}. ^{c} Covering factor of the neutral absorber. ^{d} Logarithm value of the ionization parameter (see Section 3.2). ^{e} Normalization of the power-law component, in units of 10^{-3} photons s^{-1} cm^{-2} keV^{-1}. ^{f} Flux in the 2-10 keV energy range, corrected for the Galactic absorption, in units of 10^{-11} erg cm^{-2} s^{-1}. ^{g} Intrinsic 2–10 keV luminosity, in units of 10^{43} erg s^{-1}. ^{h} This parameter was kept tied in the two states.

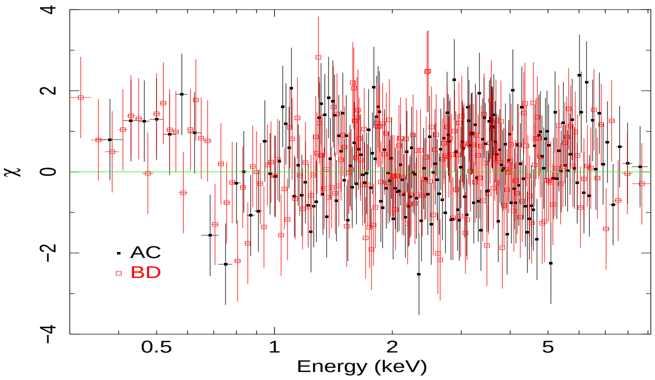

Figure 4. Residuals, plotted in terms of sigmas with error bars of size one, obtained by fitting the low- (AC) and high-state (BD) spectra of Mrk 915 with the following model: *phabs*×(*zphabs*×*zpcfabs*×*zpowerlw*).

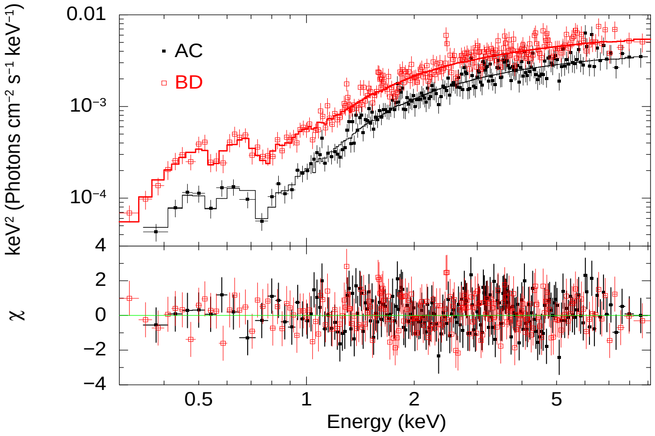

Figure 5. Upper panel: The model including an ionized absorber partially covering the source (*phabs*×(*zphabs*×*zxipcf*×*zpowerlw*)) is overplotted on the low- (AC) and high-state (BD) unfolded spectra of Mrk 915. Lower panel: Relevant residuals, plotted in terms of sigmas with error bars of size one.

these structures is expected to affect also the X-ray emission with a column density of the order of 10^{21} cm^{-2}, assuming a Galactic dust-to-gas ratio of E$_{B-V}/N_{\rm H}$=1.7×10^{-22} mag cm^2 (Bohlin, Savage, & Drake 1978). In the fitting procedure, we allowed this component to vary in the range of 0.5–5×10^{21} cm^{-2}. The third component is a neutral absorber partially covering the central source (*zpcfabs* model in XSPEC), associated with material on the torus distance scale. The full parametrization adopted is the following one: *phabs× (zphabs×zpcfabs×zpowerlw)*. We allowed to vary the intrinsic power-law normalization and both the intrinsic column density and the covering factor of the partial covering absorber. The residuals between the data and the best-fitting model for the two states are shown in Fig. 4.

Although this model can account for most of the data, it leaves evident and systematical residuals in the softer part of the spectra: by considering the data in the 0.3–1 keV range we found χ^2/ d.o.f.=55.42/37 (corresponding to a null hypothesis probability of ∼3 per cent). Thus, this model can not be considered a good representation of the global spectral properties of the source. In particular, the shape of the residuals in Fig. 4 suggests the presence of an absorption trough at ∼0.78 keV (observed frame); at the redshift of the source, this feature could be associated with Fe XVII- XVIII, typically observed in nearby bright AGN with warm absorbers (Crenshaw, Kraemer, & George 2003; Porquet et al. 2004). Prompted by these considerations, we replaced the neutral partial covering component with an ionized one, modelled in XSPEC with *zxipcf* (Reeves et al. 2008). In this case, the full parametrization is the following: *phabs× (zphabs×zxipcf×zpowerlw)*. As a first step, in the fitting procedure, we left the intrinsic $N_{\rm H}$, the ionization parameter ξ[7] and the covering factor (CF) of the ionized medium free to vary, along with the intrinsic power-law normalizations ($A_{\rm p}$). The best-fitting values obtained in the presence of an ionized absorber are reported in Table 2, where the uncertainties are given at the 90 per cent confidence level for one parameter of interest (Avni 1976). The unfolded spectra and the ratio between data and best-fitting

---

[7] The ionization parameter is defined as ξ[erg cm s^{-1}]= $L_{\rm ion}/nR^2$ (Tarter, Tucker, & Salpeter 1969), where $L_{\rm ion}$ is the ionization luminosity obtained by integrating the X-ray intrinsic luminosity between 0.013 and 13 keV, n is the average absorber number density [part/cm^{-3}] of the illuminated slab, and R is the distance of the absorber from the central source.

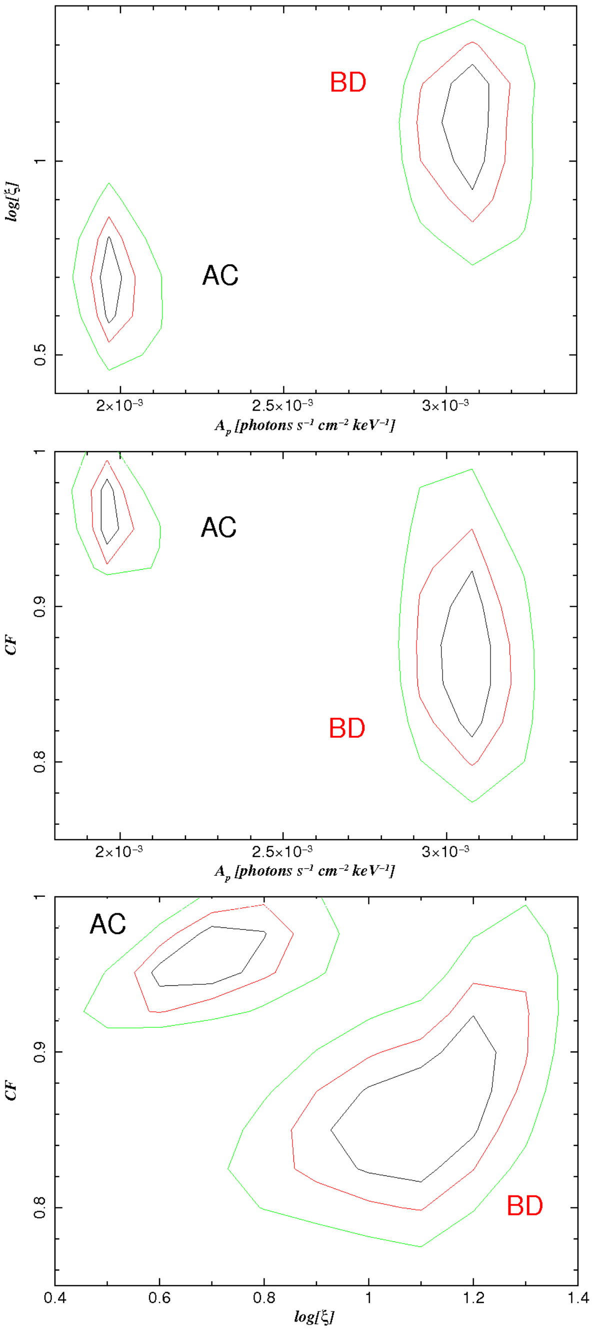

Figure 6. 68 per cent, 90 per cent and 99 per cent confidence contours for the AC state and BC states for different parameters of interest obtained by using the model reported in Table 2. Top panel: ionization state versus the power–law normalization ($A_{\rm p}$). Middle panel: Covering factor versus the power–law normalization ($A_{\rm p}$). Bottom panel: Covering factor versus the ionization state.

models are shown in Fig. 5; it is evident that this second model provides a better characterization of the spectra of Mrk 915, also in the softer energy range (χ^2/d.o.f.=22.42/35 in the 0.3–1 keV range, corresponding to a null hypothesis probability of $\sim$95 per cent). Also the residuals at $E\sim$0.78 keV are now well reproduced. We note that, with the present data, we cannot investigate the presence of a possible outflow velocity. Thus, the *redshift* of the ionized absorber was fixed to the same z of the source.

The confidence contour plots of the joint errors for different parameters of interest (log(ξ), CF and $A_{\rm p}$), obtained with the same choices of fixed parameters as quoted in Table 2, are shown in Fig. 6. The emerging scenario is that, in both states, the nucleus is obscured by a variable ionized medium with an $N_{\rm H}$ of the order of 2×10^{22} cm^{-2} and a significant increase in the power-law normalization by a factor of $\sim$1.5 from the low- (AC) to the high-state (BD) is also required (see Table 2). We note that, this increase is required also in the case of neutral partial covering absorber. In combination with an intrinsic fading/increasing of the power–law normalization, Fig. 6 suggests also a marginally evidence for a change of the ionization state and of the CF, albeit with low significance. In particular, when the source gets brighter the ionization state tentatively increases (90 per cent confidence level, see Fig. 6, top panel) and the CF slightly decreases (68 per cent confidence level, see Fig. 6, middle panel).

In the bottom panel of Fig. 6, we report the confidence contour plot of the joint errors of the CF versus the ionization parameter. This plot indicates that our spectra could be equally reproduced by assuming that only one of these two parameters is changing. Thus, we re-fitted the data twice, forcing the two spectral states to have: (1) the same ionization parameter, allowing the CF to be free to vary, and, (2) the same CF, allowing the ionization parameter to be free to vary. As expected, in both the cases we were able to reproduce our spectra with a statistical quality similar to that reported in Table 2 and showed in Fig. 5. In both cases, the intrinsic column density for the ionized medium ($N_{\rm H}\sim2\times10^{22}$ cm^{-2}) and the change in the power-law normalization (by a factor of 1.5) are consistent with the values previously obtained.

In the case in which the two ionization parameters were tied together (log(ξ)=0.63$\pm$0.15), the spectral shape variation could be completely ascribed to a change in the CF from $\sim$0.97 in the low-spectral state to $\sim$0.85 in the high-spectral state (χ^2/d.o.f.=365.33/404). In the case with the two covering factors tied together (CF=0.95$\pm$0.03), the spectral shape variation could be completely ascribed to a change in the log(ξ) from $\sim$0.77 in the low-spectral state to $\sim$1.35 in the high-spectral state (χ^2/d.o.f.=363.5/404).

Finally, we tested the picture discussed above fitting our final model, with both hypotheses of constant ξ or constant CF, to the single spectra showed in Fig. 3 (i.e. A, B, C, and D spectra spaced by about 5×10^5 s, see Fig. 1). We found results consistent with those previously described. In spite of the lower statistics of the data with respect to the combined spectra, the variations in the ξ and CF parameters still remains statistically significant (68–90 per cent confidence level) as the change in the power-law normalizations (more than 99 per cent confidence level).

4 DISCUSSION

The spectral analysis performed on the XRT monitoring data of Mrk 915 unveiled the presence of an ionized absorber with $N_{\rm H}$ of the order of 2×10^{22} cm^{-2} and allowed us to detect a variability of the intrinsic power of the central source of a factor of $\sim$1.5 on a time-scale of a few days. The possibility that the source could intrinsically decrease/increase its power was already suggested from observations in the optical domain (see Section 2 for relevant references).

As for the spectral variation observed in the X-ray domain, we found that it could be due to a change in the ionization state of the circumnuclear medium and/or to a change of the covering of absorbing medium along the line of sight. Higher quality data are needed to understand if only one or both these parameters actually vary. If the variation of the covering factor will be confirmed, this implies a clumpy structure of the absorber. Since our X-ray data can not firmly confirm or discard this hypothesis, in the following we discuss some constraints on the location of the absorber by assuming both a homogeneous and a clumpy medium.

Homogeneous medium. Under the hypothesis of homogeneous medium, we can place an upper limit on the location of this absorber by using the relation between the intrinsic continuum luminosity, the ionization and the density of the medium: $\xi = L_{\rm ion}/nR^2$. Assuming that the thickness of the absorber is less than the distance from the central SMBH (ΔR/R$<$ 1), this relation provides an upper limit on its distance: $R<L_{\rm ion}/N_{\rm H}\xi$. From the X-ray spectral analysis we derived: $N_{\rm H}\sim2\times10^{22}$ cm^{-2} and $L_{\rm ion}$=(2.4–3.7)$\times10^{43}$erg s^{-1} (low-high state, respectively; $L_{\rm ion}$ is the intrinsic X-ray luminosity, corrected for absorption, and integrated between 0.013 and 13 keV, see also footnote 7). By considering the minimum value of ξ obtained under the hypothesis of no covering factor variation, we obtain $R<(2$–$3)\times10^{20}$ cm, i.e. lower than (0.8–3)$\times10^{7}$ $R_{\rm g}$ ($R_{\rm g}$=$GM_{\rm BH}/c^2$ is the gravitational radius, where $M_{\rm BH}$ is the SMBH mass equal to 0.6-1.8$\times10^{8}$ M$_{\odot}$; Bennert et al. 2006). This estimate corresponds to a location inside the outer edge of the torus.

Clumpy medium. Under the hypothesis of a clumpy medium and assuming that the absorber is composed by spherical gas clouds moving around the central source with Keplerian velocity (e.g. Risaliti et al. 2002, Elvis et al. 2004, Risaliti et al. 2005), the variability time-scale between the two maxima (B and D) detected in Fig. 1 and Fig. 2, $<t>=10^6$ s, at the first order, is equal to the crossing time for a single cloud through the source.

The distance $R_{\rm c}$ of the absorber from the central source is given by: $R_{\rm c}$=$GM_{\rm BH}$ $t_{\rm c}{}^2$ / $(D_{\rm s}+D_{\rm c})^2$ where $t_{\rm c}$ is the variability time and $D_{\rm c}$ and $D_{\rm s}$ are the cloud and central source linear size, respectively. Under the hypothesis that the linear size of a single cloud is of the same order of that of the emitting central source, and taking into account that $D_{\rm c}$=$N_{\rm H,c}/n_{\rm c}$, we can re-write the distance $R_{\rm c}$ in the following way: $R_{\rm c}$= 0.25 $GM_{\rm BH}$ $t_{\rm c}{}^2 n_{\rm c}{}^2$ $N_{H,{\rm c}}{}^{-2}$, i.e., for $N_{\rm H,c}$=2$\times10^{22}$ cm^{-2}:

$$R_{\rm c} \sim 5 - 15\ n_{\rm c}^{2}\ {\rm cm} \qquad (1)$$

The range of values reported in equation (1) is due to the uncertainty in the $M_{\rm BH}$ (0.6–1.8$\times10^8$ M$_{\odot}$, see Section 2).

A conceptually different estimate of $R_{\rm c}$ can be derived from the relation quoted above between the intrinsic continuum luminosity, the ionization parameter and the density of the absorber ($\xi = L_{\rm ion}/n_{\rm c}R_{\rm c}^2$). By considering an average value of the ξ parameter of 10 erg cm s^{-1} and of the intrinsic ionization luminosity of $L_{\rm ion}\sim3\times10^{43}$ erg s^{-1}, we can derive:

$$R_{\rm c} = (3\times10^{42} n_{\rm c}^{-1})^{1/2}{\rm cm}. \qquad (2)$$

By combining the results reported in (1) and (2), we find that, under the hypothesis of absorbing clouds with linear dimension similar to that of the central source, the clumpy medium should be located at a distance $R_{\rm c}$=(1.4–1.7)$\times10^{17}$ cm (i.e. $\sim10^4R_{\rm g}$), with an average cloud density of $n_{\rm c}\sim$(1–1.7)$\times10^8$ cm^{-3} and an average linear dimension of $D_{\rm c}\sim D_{\rm s}\sim$(1–1.2)$\times10^{14}$ cm (i.e. $\sim7R_{\rm g}$).

We repeated the estimates discussed above by taking into account that the linear size of the single cloud could indeed be smaller (e.g. $D_{\rm c}\sim0.5$ $D_{\rm s}$) or greater ($D_{\rm c}>>D_{\rm s}$) with respect to that of the central source. We found that $R_{\rm c}$ could vary between $\sim10^{17}$ cm and 2.2$\times10^{17}$ cm with a density $n_{\rm c}$ between 2.2$\times10^8$ cm^{-3} and 6$\times10^7$ cm^{-3}, respectively.

By considering the 5100$\mathring{A}$ luminosity estimated by Bennert et al. (2006) for this source ($\lambda L_\lambda\ \sim\ 1.68\times10^{44}$ erg s^{-1}) and the relation found by Bentz (2009) between the BLR size and the 5100$\mathring{A}$ luminosity, the BLR in Mrk 915 is expected to be located at a distance from the centre SMBH of the order of 10^{16}– 10^{17} cm. If confirmed, the short time-scale variation of the CF would imply that the ionized absorber clouds should be located near, or just outside, to the bulk of the BLR with a density between 6$\times10^7$ and 2.2$\times10^8$ cm^{-3}. This range of densities would indeed be consistent with the expected lower limit of the electron density for the BLR ($n_{\rm c}$(BLR)$>10^8$ cm^{-3}; Osterbrock 1989). We note that this scenario is very similar to that proposed by Goodrich (1995), see Section 2, to explain the optical variability of this source.

5 SUMMARY AND CONCLUSIONS

From the optical point of view, Mrk 915 is a spiral galaxy hosting an intermediate (type 1.5–1.9) AGN with evident dust lane structures crossing the central source. Significant variability (about a factor of 2.5–3) in the intensity of both the broad component of the Hα emission line and the underlying continuum has been observed and reported in the literature on time-scale of few years. The analyses carried out by different authors suggest that this change could be due to an increasing of the reddening along the line of sight, to a fading of the central source, or to a combination of them. Thanks to the unique capabilities of XRT on-board the *Swift* satellite, it was possible to investigate the daily time-scale variation of the X-ray absorber.

As discussed in Section 1, Mrk 915 was selected as a good candidate for a variable absorber on the basis of the X-ray colour analysis on archival XRT data. The analysis of these observations (Ballo et al. 2015), which caught the source in two different states, suggested that this could be associated with a variable absorber.

With the aim at obtaining higher quality data on shorter time-scale, we performed a XRT monitoring covering $\sim$3 weeks and sampling days time-scale. During these new observations the source was caught again in two main different count rate and spectral states. We investigated the nature of the variable absorber testing two partial covering models: in the first one the absorber is neutral, while in the second one it is ionized. In both cases, we added a neutral absorber ($N_{\rm H}\sim10^{21}$ cm^{-2}) associated with the dust lanes structures seen crossing the central source. We find that, while the first model (neutral absorber) is not able to reproduce the data below 1 keV, the second one (ionized absorber) provides a good characterization of the data in the full energy range considered here. Furthermore, we detect a significant variation of the intrinsic power of the nuclear source. The quality of the present data prevents us from firmly establishing if the observed spectral variations were due to a change in the ionization state of the circumnuclear medium and/or to its covering factor. Higher quality data are needed to establish if only one or both of these parameters change in this source. By combining the information provided by the X-ray light curve and by the spectral analysis, we derived some constraints on the absorber location under the hypothesis of a homogeneous and a clumpy medium. In both cases, the absorber should be located inside the outer edge of an extended torus and, in particular, under the clumpy hypothesis, it should be located close, or just outside, to the BLR zone.

ACKNOWLEDGMENTS

This work is based on observations obtained with the *Swift* satellite and it made use of data supplied by the UK *Swift* Science Data Centre at the University of Leicester. We thank Neil Gehrels, Boris Sbarufatti, Gianpiero Tagliaferri and the *Swift* Mission Operation Center to make every effort to get our ToO request scheduled. This research has made use both of the Palermo BAT Catalogue and database operated at INAF - IASF Palermo and of the 70 month *Swift*-BAT Catalogue. We, moreover, thank Miguel Perez-Torres for the analysis of archival VLA data. Part of this work was supported by the European Commission Seventh Framework Programme (FP7/2007-2013) under grant agreement no. 267251 Astronomy Fellowships in Italy (AstroFIt). The authors acknowledge financial support from the Italian Ministry of Education, Universities and Research (PRIN2010-2011, grant no. 2010NHBSBE). Support from the Italian Space Agency is acknowledged (contract ASI INAF I/037/12/0). Finally, we you would like to thank the anonymous referee for the useful and constructive comments which improved the quality of the paper.

REFERENCES

Antonucci R., 1993, ARA&A, 31, 473

Avni Y., 1976, ApJ, 210, 642

Ballo L. et al., 2015, ed. by P. Caraveo, P. D'Avanzo, N. Gehrels and G. Tagliaferri; Proc. of "Swift: 10 years of discovery", 2-5 December 2014, Rome, Italy; Proceedings of Science (PoS, Trieste, Italy), vol. SWIFT 10, PoS(SWIFT10)122 (arXiv:1505.02593)

Baumgartner W. H., Tueller J., Markwardt C. B., Skinner G. K., Barthelmy S., Mushotzky R. F., Evans P. A., Gehrels N., 2013, ApJS, 207, 19

Bennert N., Jungwiert B., Komossa S., Haas M., Chini R., 2006, A&A, 459, 55

Bentz M. C., Peterson B. M., Netzer H., Pogge R. W., Vestergaard M., 2009, ApJ, 697, 160

Bianchi S., Maiolino R., Risaliti G., 2012, Adv. Astron., 2012, 782030

Bohlin R. C., Savage B. D., Drake J. F., 1978, ApJ, 224, 132

Braito V., Reeves J. N., Gofford J., Nardini E., Porquet D., Risaliti G., 2014, ApJ, 795, 87

Burrows D. N., et al., 2005, Space Sci. Rev., 120, 165

Connolly S. D., McHardy I. M., Dwelly T., 2014, MNRAS, 440, 3503

Crenshaw D. M., Kraemer S. B., George I. M., 2003, ARA&A, 41, 117

Cusumano G. et al., 2010, A&A, 524, A64

Elvis M. Risaliti G., Nicastro F., Miller J. M., Fiore F., Puccetti S., 2004, ApJ 615, L25

Evans P. A. et al., 2007, A&A, 469, 379

Evans P. A. et al., 2009, MNRAS, 397, 1177

Goodrich R. W., 1995, ApJ, 440, 141

Kalberla P. M. W., Burton W. B., Hartmann D., Arnal E. M., Bajaja E., Morras R., Pöppel W. G. L., 2005, A&A, 440, 775

Keel W. C., 1996, ApJS, 106, 27

Malkan M. A., Gorjian V., Tam R., 1998, ApJS, 117, 25

Moretti, A. et al. 2005, in Siegmund O. H. W., ed., Proc. SPIE Conf. Ser. Vol. 5898, UV, X-ray, and Gamma-Ray Space Instrumentation for Astronomy XIV. SPIE, Bellingham, p. 360

Muñoz Marín V. M., González Delgado R. M., Schmitt H. R., Cid Fernandes R., Pérez E., Storchi-Bergmann T., Heckman T., Leitherer C., 2007, AJ, 134, 648

Osterbrock D. E., 1989, Sky Telesc., 78, 491

Porquet D., Reeves J. N., O'Brien P., Brinkmann W., 2004, A&A, 422, 85

Reeves J., Done C., Pounds K., Terashima Y., Hayashida K., Anabuki N., Uchino M., Turner M., 2008, MNRAS, 385, L108

Risaliti G., Elvis M., Nicastro F., 2002, ApJ, 571, 234

Risaliti G., Elvis M., Fabbiano G., Baldi A., Zezas A., 2005, ApJ, 623, L93

Risaliti G., Elvis M., Fabbiano G., Baldi A., Zezas A., Salvati M., 2007, ApJ, 659, L111

Risaliti, G., Salvati, M., Elvis, M., Fabbiano, G., Baldi, A., Bianchi, S., Braito, V., Guainazzi, M., Matt, G., Miniutti, G., Reeves, J., Soria, R., Zezas, A., 2009, MNRAS 393, L1

Tarter C. B., Tucker W. H., Salpeter E. E., 1969, ApJ, 156, 943

Trippe M. L., Crenshaw D. M., Deo R. P., Dietrich M., Kraemer S. B., Rafter S. E., Turner T. J., 2010, ApJ, 725, 1749

Whittle M., 1992, ApJS, 79, 49